LA-UR-14-25447
Approved for public release; distribution is unlimited.

Title: Corrosion mechanisms for metal alloy waste forms – experiment and theory Level 4 Milestone M4FT-14LA0804024 Fuel Cycle Research & Development

Author(s): Liu, Xiang-Yang
Taylor, Christopher D.
Kim, Eunja
Goff, George Scott
Kolman, David Gary

Intended for: Report

Issued: 2014-07-31 (rev.1)

Corrosion mechanisms for metal alloy waste forms – experiment and theory
Level 4 Milestone M4FT-14LA0804024
Fuel Cycle Research & Development

Prepared for U.S. Department of Energy
Used Fuel Disposition Campaign

X.-Y. Liu[1], C. D. Taylor[2], E. J. Kim[3], G. Goff[1], D. Kolman[1]
[1]Los Alamos National Laboratory
[2]Fontana Corrosion Center, Ohio State University
[3]University of Nevada – Las Vegas

July 11, 2014

Level 4 Milestone: Corrosion mechanisms for metal alloy waste forms – experiment and theory
Milestone ID: M4FT-14LA0804024
Due Date: 7/11/2014

Deliverables:

Report will be produced, with signed coversheet of peer-reviewer and distributed to David Sassani, Joe Price, Kevin McMahon, Peter Swift, Bill Ebert, Louise Criscenti.

Date deliverable met:

7/11/2014

SUMMARY

This document meets Level 4 Milestone: Corrosion mechanisms for metal alloy waste forms – experiment and theory. A multiphysics model is introduced that will provide the framework for the quantitative prediction of corrosion rates of metallic waste forms incorporating the fission product Tc. The model requires a knowledge of the properties of not only the metallic waste form, but also the passive oxide films that will be generated on the waste form, and the chemistry of the metal/oxide and oxide/environment interfaces. In collaboration with experimental work, the focus of this work is on obtaining these properties from fundamental atomistic models. Herein we describe the overall multiphysics model, which is based on MacDonald's point-defect model for passivity. We then present the results of detailed electronic-structure calculations for the determination of the compatibility and properties of Tc when incorporated into intermetallic oxide phases. This work is relevant to the formation of multi-component oxides on metal surfaces that will incorporate Tc, and provide a kinetic barrier to corrosion (i.e. the release of Tc to the environment). Atomistic models that build upon the electronic structure calculations are then described using the modified embedded atom method to simulate metallic dissolution, and Buckingham potentials to perform classical molecular dynamics and statics simulations of the technetium (and, later, iron-technetium) oxide phases. Electrochemical methods were then applied to provide some benchmark information of the corrosion and electrochemical properties of Technetium metal. The results indicate that published information on Tc passivity is not complete and that further investigation is warranted.

TABLE OF CONTENTS

1. OBJECTIVES AND SCOPE OF WORK

The development of advanced waste forms for disposition of fission products, particularly technetium, requires a science-based approach to the prediction of their resistance to environmental degradation. In the case of metallic alloy waste forms, the fundamental degradation mechanism is via corrosion. Although the corrosion properties of technetium alloy waste forms can be simulated by electrochemical testing, a fundamental understanding, pertinent to performance over geological timeframes, can be obtained using deterministic, *ab initio* models. The objectives of this project are currently focused on understanding the corrosion mechanisms for metal alloy waste forms, including obtaining a detailed model of the passivation properties, by simulating the oxide films that form on candidate alloy waste forms comprised primarily of Fe, Mo, Cr and Tc.

Considering the difficulties in obtaining accurate experimental measurements of both the early stages of oxidation and the extremely long-term corrosion properties of Tc alloy waste forms, the approach we have adopted relies heavily on modeling. In this milestone report, we first propose a predictive multistep model for the release of Tc from passive metal alloy waste forms, based on the general scheme for passive oxide films. Following this model, we also lay out how density functional theory will be applied to predict the kinetic parameters associated with the relevant migration processes. Next, we report the density functional theory modeling of Tc incorporation and transport in intermelallic oxides. We started by reviewing prior work on binary Tc oxides. Then report spin-polarized DFT results of Tc incorporation and diffusion in FeO, Fe_2O_3, and Fe_3O_4 under dilute limit cases. To understand the waste form stability in different spinel

lattices, we also studied the Tc concentration dependence on the stability of different Tc containing spinel Fe oxides. Additionally, based on our earlier success in kinetic Monte-Carlo modeling, we also compared Tc alloy corrosion behaviors in Tc-Fe, Tc-Mo, and Tc-Ni alloys. To enable the passive film modeling via large scale molecular dynamics simulations, we optimized Buckingham potential for Tc-O interaction for TcO_2 oxide. For the electrochemical characterization experiments, we carried out the electrochemical corrosion test on pure Tc in pH 3.2 H_2SO_4, and reporting the non-passive film formed on pure Tc under electrochemical testing conditions. Finally, we summarize our findings and provide perspectives.

2. MODELING OF METALLIC WASTE FORMS FROM FIRST-PRINCIPLES BASED APPROACHES

2.1. *Predictive multistep model for the release of Tc from passive metal alloy waste forms*

2.1.1. Motivation

One pathway under consideration for spent nuclear fuel is to separate the various fission products and remaining fuel elements using electrochemical pyrolysis. The separated metals, including technetium (Tc) could then be alloyed together to form stainless ingots, engineered to resist corrosion over long time scales.[1, 2] The resistance of stainless metal alloys to corrosion is imparted by the formation of oxide scales that have extremely slow transport kinetics, thus constraining the rate at which material from the bulk of the alloy can interact with the environment.[3] Using electrochemical testing, it is possible to examine the corrosion properties of candidate metal alloy waste forms under conditions such as variable composition, temperature or chemical exposure.[4] Necessarily, experiments are constrained to relatively short testing times and a small number of possible materials/environment combinations. For this reason, it is helpful to also develop a comprehensive model based on first-principles that can be reliably applied to screen a variety of possible materials and environment combinations. The model can be used for the purposes of prediction of corrosion rates, design of alloys, and to provide fundamental insights that will complement the experimental synthesis and characterization of these candidate alloy waste forms.

In the present report we describe the multistep corrosion mechanism that is responsible for the release of Tc from any candidate alloy waste form, and outline the

first-principles approach that will be used to build a predictive model for candidate alloy waste form corrosion, useful for both alloy design, and making long-term predictions.

2.1.2. The multistep corrosion mechanism

The dissolution of Tc alloy waste forms will follow a multistep corrosion mechanism, following the general presentation made by MacDonald's point-defect model for passive oxide films,[5-7] as shown in Figure 1.

Metal/Oxide interface:

(a) $$Tc_m + V_M^{\chi'} \overset{k_1}{\rightarrow} Tc_M + V_m + \chi e' \quad (1)$$

Transport of a metallic Tc atom into a cation vacancy site in the oxide film, leaving a vacancy in the metal site and releasing electrons (oxidation)

(b) $$Tc_m \overset{k_2}{\rightarrow} Tc_M + (\tfrac{\chi}{2})V_{\ddot{O}} + \chi e^- \quad (2)$$

Conversion of a metal atom site into a cation site, with creation of an accompanying oxide vacancy and release of electrons (oxidation).

Transport of defects in the oxide:

(c) $$Tc_M \overset{k_3}{\rightarrow} Tc_{(aq)}^{4+} + V_M^{\chi'} + (4-\chi)\, e' \quad (3)$$

Migration of technetium cations through the oxide film. Possibly with interchange with Fe, Cr or Mo cations depending on the composition and activation barriers.

(d) $$V_{\ddot{O}} + O_O \overset{k_4}{\rightarrow} O_O + V_{\ddot{O}} \quad (4)$$

Migration of oxide anions through the oxide.

Oxide/Environment interface:

(e) $$Tc_M \overset{k_5}{\rightarrow} Tc_{(aq)}^{4+} + V_M^{\chi'} + (4-\chi)\, e' \quad (5)$$

Dissolution of the metal cation from the oxide surface into solution.

(f) $V_{\ddot{O}} + H_2O \overset{k_6}{\rightarrow} O_O + 2H^+$ (6)

Uptake of oxygen into the vacancy sites at the oxide lattice from water.

(g) $MO_{\chi/2} + \chi H^+ \overset{k_7}{\rightarrow} Tc^{4+}_{(aq)} + \frac{\chi}{2}H_2O + (4-\chi)e'$ (7)

Dissolution of the metal oxide via acid-base reaction between the oxide base and acid in solution.

The relative rates k_1, k_2, k_3, k_4, k_5, k_6 and k_7 and their interdependence will determine the steady state corrosion rate of the metal alloy waste form. The slowest rate will represent the rate-determining step that will control the overall corrosion process. The rates will also be a function of the open circuit potential (OCP).

A combination of experiment and theory will be used to establish the mechanism and provide information for the rate constants k_1, k_2, k_3, k_4, k_5, k_6 and k_7. As noted in the above presentation of the mechanistic steps, for alloy waste forms, there will be multiple types of cation defect site corresponding to the presence of different intermetallic phases, solid solutions and oxide structures. For example, if the film is predominantly Fe_2O_3 above an Fe solid-solution containing Tc, then the appropriate steps likely involve the migration of Tc metal as a defect in the bcc Fe lattice, into a Fe cation vacancy in the iron-oxide. Whereas if the oxide film is spinel like (Fe_2CrO_4) then, again, the appropriate crystallographic relations and point-defects will need to be considered. The candidate alloy waste forms that have been prepared to date have a multiphase composition, include some ferritic phases as well as Fe-Cr-Mo solid solutions, and thus the corrosion of the waste form will proceed according to the proportions of each phase that forms on the exterior surface of the alloy. Some other factors to consider are the requirement for charge balance, given that Fe ions are in a +2 or +3 state, whereas Tc prefers the +4 state.

Thus density functional theory calculations or classical molecular dynamics or statics will be needed to find the appropriate defect state for Tc cations in the iron-oxide or spinel lattice.

2.1.3. First-principles approach

Contemporary solid-state physics allows the prediction of crystal structures for materials of arbitrary composition, including intermetallic compounds and ceramics, with a high-degree of accuracy, using the method known as density functional theory.[8, 9] Not only can crystal structures be computed with this method, but also the structure and properties of point-defects, surfaces and transition states associated with the transport of defects and chemical reactions.[10-12] Density functional theory can be used to make these predictions because it follows the principles developed in the early 20th century for the basic quantum mechanical interactions between the atomic nuclei and the electrons that give rise to atomic structure and bonding: the principles upon which crystallography and chemical reactivity are based.[13, 14] In this section we lay out how density functional theory will be applied to predict the kinetic parameters associated with the relevant migration processes outlined in the previous section.

Characterization of point-defects

In coordination with experimental characterization efforts, the predominant crystallographic forms for the oxide films will need to be identified and the appropriate electronic structure method (i.e. exchange-correlation functional and/or self-interaction approach) selected for modeling the crystal structure of the oxide film. The two oxides that have been identified in the Alloy Waste Form effort are hematite (Fe_2O_3) and the iron-chromium spinel (Fe_2CrO_4). Based on this finding, Tc migration through the oxide

scale will occur through point-defects in both of these phases, and the total Tc migration will be a linear combination of the rate constants for these two phases based on their relative abundance in terms of fractional surface area of the alloy. Prior to modeling the kinetics of Tc transport, however, it is important to establish the equilibrium structure of Tc incorporated into these two oxide phases, and this can be performed using molecular statics: that is, using a combination of density functional theory and interatomic potentials, to determine the lowest energy (i.e. most likely) state for Tc to adopt as it substitutes for Fe (or Cr or Mo) in these oxide films, as well as to model the structure of vacancies in the vicinity of Tc, as the migration of Tc to a neighboring vacancy site is likely to comprise the transport mechanism, according to equation (3) above. Once the reactant and product states for the migration of Tc point-defects in the oxide films have been elucidated, it will then be possible to use transition state theory to model the rate at which Tc cations will migrate within the oxide film.

It is possible that Tc will transport through grain-boundaries in the oxide film, rather than as point-defects. Although it is possible to model grain-boundary transport from a first-principles standpoint, we will need to consider that possibility in a future work, since those models will build off the bulk models, and so the work outlined in the present phase would be a necessary starting point anyway.

Transport of oxide anion in the iron-rich oxide phases is not likely to differ based on Tc content, hence, rate constants available in the literature should be sufficient for modeling equation (4).

Characterization of interfaces

Reactions (a) and (b) occur at the metal/oxide interface, and reactions (e)-(g) occur at the oxide/environment interface. Previously, we have initiated models for the Tc/TcO_2 interface using density functional theory [15]. The next step is to model the Fe/FeO_x interface and the interfaces between solid-solution and intermetallic phases with the spinel Fe_2CrO_4. Similarly to the preceding section on point-defect structure, the interfaces will also possess an equilibrium structure. Using density functional theory and variable charge interatomic potentials (like ReaxFF or COMB) [16, 17], it is possible to find these equilibrium structures, and to consider how they will be perturbed by the presence of dissolved Tc. Subsequently, one can perturb these structures to examine transport processes, again, using transition state theory. In this way, the rate constants for equations (1) and (2) can be predicted.

Reactions (e) and (g) are dissolution reactions, where the Tc cation, having migrated through the oxide film then reacts with water to form the solubilized pertechnetate ion. This process can also be modeled using density functional theory, or by using suitable interatomic potentials, parameterized using density functional theory data. The models for Tc point-defects in iron oxide phases developed at PNNL will be generalized to surface states and applied to uncover the rate constants for reactions (e) and/or (g).[18]

Reaction (f) is the incorporation of oxygen from the environment into the oxide film. As with reaction (d) we do not expect this rate constant to be heavily dependent upon the presence of Tc, so we plan to use literature data for this reaction rate for the hematite and spinel phases.

Integration into a kinetic model

Once the rate constants are established, one of three predominant conditions will be revealed:

1. Cation vacancy annihilation at the metal/oxide interface is rate-limiting

If it is found that the rate constant for equation (1) or (2) is lower than the rate for diffusion across the oxide film (equation (3)) or dissolution (equation (5) or (7)) then the loss of Tc from the candidate alloy waste form will be limited by the rate at which Tc enters the passive layer. This information could then be used to investigate alloy compositions or interface engineering strategies for further decreasing this rate constant, if further optimization of this value is required.

2. Transport of Tc through the film is rate-limiting

In this case equilibrium conditions will exist at the metal/film and film/environment interfaces, and the rate at which the Tc is released into the environment will be equal to the diffusion rate across the oxide film, given by the rate constant for equation (3). We assume here that the rate of counter flow of the oxide anion in the film will not impact the rate of outward Tc migration, because other cations, such as Fe(II) and Fe(III) will predominantly be providing the necessary charge balance. Experimentally determined oxide thicknesses will be used to estimate the rate of Tc transport across the film, along with the rate constants for point-defect migration obtained from density functional theory. The rate will also depend on the concentration gradient, which we can estimate based on background Tc levels and the desired alloy composition.

3. Dissolution of Tc at the oxide/environment interface

In this condition, there will exist an equilibrium between the Tc concentrations in the alloy and the oxide film, and the limitation will come from the rate at which Tc can

dissolve from the oxide film via reactions (e) or (g). The equilibrium concentration of Tc in the oxide film can be determined from Boltzmann distribution and the formation energies for Tc point-defects in the oxide film, as well as the chemical potential of Tc in the alloy itself.

2.2. *Density functional theory modeling of Tc incorporation and transport in intermelallic oxides*

2.2.1. Computational approach

First-principles total energy calculations were performed using density functional theory (DFT) as implemented in the *Vienna ab initio simulation package* (VASP) [8]. The exchange–correlation energy was calculated using the generalized gradient approximation (GGA) with the parameterization of Perdew, Burke, and Ernzerhof (PBE) [19]. The interaction between valence electrons and ionic cores was described by the projector augmented wave (PAW) method [20]. The Tc (4p,5s,4d) electrons were treated explicitly as valence electrons in the Kohn–Sham (KS) equation and the remaining core electrons together with the nuclei were represented by PAW pseudopotentials. The plane-wave cutoff energy for the electronic wavefunctions was set to a value of 400 eV. Periodic unit cells were used to calculate the total energy of iron oxides in which Tc atoms are incorporated. Electronic relaxation was performed with the conjugate gradient method accelerated using the Methfessel–Paxton Fermi-level smearing [21] with a Gaussian width of 0.2 eV. Ionic relaxation was carried out using the Hellmann–Feynman forces acting on atoms. The Brillouin zone was sampled using the Monkhorst–Pack special k-point scheme [22] for structural optimization and total energy calculations.

2.2.2. Previous results of binary Tc oxides

In line with the efforts to develop metal alloy waste-forms that can immobilize Tc, the present research activities are focused on screening possible oxide candidates that can incorporate Tc and that can also provide insights into the surface oxide properties that are crucial for gaining fundamental understandings of the corrosion process of metal surfaces. A first attempt was made to understand possible polymorphism in the Tc-O binary system. So far, two oxides of technetium have been synthesized and characterized experimentally: (i) black-colored technetium dioxide (TcO_2) [23] and (ii) pale-yellow heptoxide (Tc_2O_7) [24, 25]. Single crystal of Tc_2O_7 was synthesized by combustion of ^{99}Tc in a stream of oxygen at 400 ^{o}C [25], which crystallizes in the orthorhombic space group (Pbca) [24]. According to Muller et al.[25], TcO_2 is stabilized in the MoO_2 structure type, which is a distorted rutile structure. A systematic study was carried out to investigate the relative structural stability of possible Tc binary oxides including TcO, TcO_2, TcO_3, and Tc_2O_7 using DFT and the results were compared with experimental data available in the literature. Figure 2 depicts the optimized crystalline structures of Tc oxides. In the case of TcO, which has not been synthesized yet, the hypothetical B1 structure - since it is the most commonly found in transition metal-monoxides [26]- was selected. The calculated lattice constants of TcO_2 are a=5.77, b=4.86, and c=5.65 Å (see Table 2.2.2), in excellent agreement with experimental values [25]. The estimated formation energy of TcO_2 in a monoclinic phase is 4.25 eV per formula unit (f.u.), which is close to the experimental value of 4.75 eV/f.u. [27].

Our DFT calculations predict that the bulk modulus of TcO_2 is 203 GPa, revealing a hardness comparable to AlN [28]. Such high hardness is due to the three-dimensional

edge and corner-sharing network of TcO_6 octahedra. In TcO_2 each edge-shared oxygen is also corner-shared with an adjacent infinite chain of edge-sharing octahedral. Tc_2O_7 is one of the few known transition metal oxides having a molecular structure in the solid state [24]. Each Tc_2O_7 molecule consists of two TcO tetrahedra sharing one oxygen atom. The van der Waals forces between Tc_2O_7 molecules play a major role in holding them together in an orthorhombic lattice. The calculated lattice constants are highly overestimated compared with experimental values, pointing out the fact that DFT may handle the weak van der Waals interactions poorly, resulting in the predicted bulk modulus of about 3 GPa. A hypothetical TcO_3 structure investigated is in the MoO_3 structure as shown in Figure 2, however, is less energetically stable than TcO_2. According the estimated formation of binary Tc oxides, TcO_2 is the most energetically favorable form, followed by Tc_2O_7.

2.2.3. Dilute Tc incorporation and diffusion in FeO, Fe_2O_3, and Fe_3O_4

As stated in previous sections, how Tc is incorporated into iron oxides is one of the most important processes in the Tc release model. In this section, spin-polarized DFT calculations were firstly attempted to understand the energetics of Tc incorporation in the vacancy defect sites for a range of iron oxides, FeO, α-Fe_2O_3, and Fe_3O_4.

Magnetism is known to play an active role in the electronic structures of these iron oxides. FeO, or wüstite, is dominant in the early stages of iron oxidation or in the formation of ultrathin films [16]. FeO has rock salt (NaCl) B1 type crystal structure. Below Néel temperature, this oxide has an antiferromagnetic ordering, denoted as AFM II [30]. In this ordering, the spin moments of Fe atoms in alternating (111) planes are anti-parallel in spin directions [31, 32]. Figure 3a describes such magnetic spin ordering

in FeO. For DFT supercell calculations that require periodic boundaries, a rhombohedral supercell is employed (see also Figure 3a).

α-Fe_2O_3, or hematite, is the most abundant phase among all of the iron oxides. Hematite has hexagonal corundum (α-Al_2O_3) type structure, with space group $R\bar{3}c$. The complete hexagonal unit cell of hematite is used in the DFT calculations. Below Néel temperature, this oxide also has an antiferromagnetic ordering. As noted [33], there are two types of Fe-Fe pairs in this oxide, with one type (denoted as type A) shorter, and another type (denoted as type B) larger in distance. The minimum energy state corresponds to AF + + - - state, that atoms belonging to type A pairs have equal magnetic moments while atoms belonging to type B pairs have opposite magnetic moments. This result agrees with recent other DFT calculations [34]. Figure 3b describes the magnetic spin ordering and the crystal structure in the hexagonal supercell.

Finally, Fe_3O_4, or magnetite, is the basic oxide form during early oxidation stage of stainless steel [35]. It has a cubic inverse spinel structure, with space group $Fd\bar{3}m$. In Figure 3c, such structure is shown. In the cubic unit cell, the tetrahedral sites are occupied by Fe^{3+} ions, while the octahedral sites are occupied by equal number of Fe^{3+} and Fe^{2+} ions. The Fe ions belonging to the tetrahedral sites and octahedral sites have opposite magnetic moments, so magnetite is a ferrimagnetic oxide.

Under dilute limit, it is reasonable to assume that the thermally generated or natural grown crystal oxides have enough vacancies for Tc accommodation. The DFT results for a simple Fe vacancy in three oxides, as well as the Tc incorporation energy at the available Fe vacancy sites in these oxides are summarized in Table 2.2.3. DFT results show that it will cost 3.1 eV for Tc to be incorporated at Fe vacancy in FeO. While in α-

Fe_2O_3, the Tc incorporation will release 3.1 eV in energy, making this process energetically preferred. In Fe_3O_4, while it is energetically preferred for Tc to be incorporated in octahedral Fe vacancy site, this type of vacancy site is less possible to exist due to the extremely high energetics (relative to the tetrahedral vacancy site). Further study is needed to include the strong-electron correlation effect (see section 2.2.5) to validate our findings.

Next, spin-polarized DFT calculations were carried out to obtain the migration energy barriers during diffusion, assuming that Tc is already incorporated in α-Fe_2O_3. The nudged elastic band method is used in DFT calculations [36]. Figure 4 illustrates one of the most possible diffusion pathway in α-Fe_2O_3, i.e, the type A pairs channel. For the first time, the migration energy barrier is calculated by DFT, with Tc migration via vacancy mechanism to be 1.9 eV. For pure Fe migration, the migration energy barrier is also calculated, 1.1 eV, which is substantially lower than the Tc migration. The DFT results suggest that Tc diffusion in hematite oxide is much slower than the anion (O) or cation (Fe) diffusion.

2.2.4. Waste form stability of different spinel phases

The long-term corrosion characteristics depend upon the phase-stability of the material, the nature of the passive oxide films that form on their surface, and the reactivity of the metal surfaces and oxide surfaces toward their local environment [37]. Due to the superior physicochemical properties, oxide spinel systems have been used in electrical, optical, mechanical, and magnetic applications [38]. Recently an attempt to synthesize $TcCo_2O_4$ was made successfully by Thorogood et al. [39]. The implication of this success is rather significant since this demonstrates the possibility to use spinels as

surrogate hosts for Tc incorporation. We have explored in this study the possibility to incorporate Tc in existing iron oxides in spinel (or magnetite, Fe_3O_4), calcium ferrite ($CaFe_2O_4$), and rare-earth iron oxide (YFe_2O_4) lattices. These structures are selected here for the following reasons: They are stable in (i) the same stoichiometry Tc:Fe:O=1:2:4 and (ii) the three distinct lattice types (see Figure 5a-c). In addition, the high-pressure spinel structure is isostructural with the $CaFe_2O_4$ phase or vice versa [40]. $CaFe_2O_4$ crystallizes in the orthorhombic *Cmcm* space group (see Figure 5b). The crystal structure of YFe_2O_4 is a rhombohedral layered structure with space group *R-3m* (see Figure 5c). It is characterized as an alternate stacking of the hexagonal Fe_2O_3 layer and the hexagonal YO layer along c-axis.

The DFT results are plotted in Figure 6, which predicts that magnetite is the most stable form to host Tc atoms up to about 33%, forming a $TcFe_2O_4$ spinel. Above 33 % of Tc inclusion a $TcFe_2O_4$ spinel becomes energetically less stable than the ones in $CaFe_2O_4$ and YFe_2O_4 lattices. For these high Tc concentrations, the rhombohedral phase is becoming most stable form.

2.2.5. Benchmark of strong-electron correlation effect

The benchmark calculation was carried out for magnetite (Fe_3O_4) by varying the effective strong-electron correction parameter, U_{eff}, to correct for the lack of electron localization within the framework of standard DFT. The results are compared to experimental data, as summarized in Table 2.2.5. The estimated lattice constant is underestimated when U_{eff} = 0 eV while it is slightly overestimated when U_{eff} = 2 and 4 eV, compared to the experimental value of 8.39 Å. The volume compression data also show that the calculated volume is consistently overestimated when the U_{eff} value is

greater than or equal to 1, as shown in Figure 7. This finding indicates that the LDA+U correction may be necessary to predict the structural properties of Tc incorporated iron oxides more accurately.

2.3 Atomistic scale modeling of Tc corrosion

2.3.1 kMC modeling of Tc alloy corrosion

The modified embedded atom method has been applied to enable off-lattice kinetic Monte Carlo simulations of the active dissolution of binary alloys [42]. Application of this method to the Tc-Fe, Tc-Mo, and Tc-Ni binary systems has provided some fundamental science inputs to the development of waste forms for fission products, which would otherwise be difficult to determine from a purely experimental standpoint. The kinetic Monte Carlo method provides a means for evaluating the types and relative severity of corrosion that such waste forms may experience as a function of composition, crystallography and surface orientation. Modeling of the alloy surface corrosion rate is particularly important for localized corrosion behaviors (the rupture of oxide films by localized dissolution, mechanical damage, or presence of deleterious chemistries).

In Figure 8, the corrosion morphologies of the above candidate alloy waste forms containing 1, 5 and 10 percent Tc are shown. While the corrosion morphology for Tc-Fe and Tc-Mo alloys are similar, the crystallographic pitting for Tc-Ni is sharper than Tc-Fe or Tc-Mo. Such morphology difference may suggest that the local ordering within alloy can play a significant role in the stability of the waste form.

In Figure 9, the relative corrosion rates versus Tc composition for Tc-Fe, Tc-Mo, and Tc-Ni are shown. The corrosion rate is determined from the inverse of the time

required to complete the simulation, multiplied by the number of atoms dissolved. A corrosion potential of 0 V on the hydrogen electrode scale was assumed for the simulations, at room temperature. As shown in Figure 9, regarding bcc Fe and Mo solid solutions containing Tc, the Tc addition up to 10% decreases the corrosion rate. However, such trend is reversed for fcc Ni solid solutions containing Tc up to 10%. This is presumably due to the large lattice mismatch of Tc and large dilute heat of solution (1 eV/atom) in fcc Ni.

2.3.2 Development of TcO_2 oxide empirical potential for molecular dynamics simulation

Development of reactive force fields for molecular dynamics (MD) simulations of Tc transport between metal alloys and associated oxides are desired. The main advantage of MD simulations is the much larger length scale in simulations compared to that in DFT, to treat microstructural effect such as interface misfit, grain-boundaries, etc.

As a first step toward optimization of the empirical potential parameterization, the Buckingham pair potential scheme is chosen. Buckingham type potential has been used widely for modeling a range of oxides including UO_2. The potential consists

$$E = Ae^{-r/\rho} - \frac{C}{r^6} \quad (8)$$

and the Coulombic energy, where A, ρ, and C are parameters. The optimized Buckingham potential for Tc-O interaction is fitted to the DFT calculated lattice constants and bulk modulus of TcO_2. The potential has a fixed charge model, with the charge of Tc set to +4 and O to -2 in the model. The calculated lattice constants of TcO_2 are a=7.11, b=5.01, and c=6.11 Å, compared to DFT results, a=5.77, b=4.86, and c=5.65 Å. The calculated bulk modulus of TcO_2 is 218 GPa, compared to DFT result of 203

GPa. The complex bonding of TcO_2 is modestly captured by the Buckingham potential. More complicated forms such as variable charge interatomic potentials (like ReaxFF or COMB) [16, 17] are expected to generate better empirical potential models. Currently, we are actively testing the Fe-O potential model in ReaxFF to build more experience.

3. ELECTROCHEMICAL CORROSION STUDIES FOR MODELING METALLIC WASTE FORM RELEASE RATES

Metal waste forms are being studied as possible disposal forms for technetium and other fission products from advanced nuclear fuel cycle options. In recent years, a variety of studies have been performed on various technetium alloy waste forms based on alloying technetium with zircaloy and / or stainless steel components. Alloying has been successful in producing lower-melting materials, however, the alloy products are composed of multiple phases having complex microstructures. Because the technetium release from these alloys is dominated by the least corrosion-resistant phase, understanding the corrosion response of these alloys involves understand the interplay of the metallurgy and corrosion behavior of the component phases. Corrosion studies of technetium metal are quite limited. As an initial step in assessing the viability of waste forms, technetium corrosion behavior was assessed.

Experimental. Tc metal was produced by thermal decomposition of NH_4TcO_4 to TcO_2 at 450 °C for 1 hr under a slow flow of Ar. The TcO_2 was converted to Tc metal in Ar - 5 % H_2 using a two-step furnace cycle (700 °C for 24 hours followed by 900 °C for 4 hours).

Specimens were mounted in epoxy and polished to 500 grit finish. The polished samples were ultrasonically cleaned in ethanol for five minutes. Crevice corrosion between the metal and the epoxy mount was not apparent following testing. The exposed metal surface area varied between 0.02 and 0.2 cm^2 depending on the individual sample.

Solutions were composed of ambiently-aerated pH 3.2 H_2SO_4. Solutions were room temperature - self-heating from radioactive decay was considered negligible. A

commercially-available, computer-controlled potentiostat was used to perform the electrochemical measurements. The electrochemical cell was a 100-mL, five-neck flask incorporating a Ag/AgCl reference electrode and a platinized-niobium mesh counter electrode. With the exception of in-situ abrasion tests, working electrodes were immersed in solution for four hours and the open circuit potential monitored. Potentiodynamic polarization tests used a scan rate of 0.1 mV/s. Electrochemical impedance spectroscopy (EIS) was performed using a 10-mV rms AC voltage signal, applied at frequencies between 100 kHz and 10 mHz using potentiostatic control. Impedance data fitting was performed using complex nonlinear least squares circuit fitting software. Most tests were replicated to assess the reproducibility of the results, with as many as eight replicate tests performed.

Results and discussion. Open circuit potential measurements are shown in Figure 10. Data are superimposed on the potential – pH diagram for Tc. The red and black lines represent two different published values for the TcO_2 / TcO_4^- transition. The open circuit potential appears to fall near or above the transition. The TcO_4^- region is a region of corrosion (as opposed to passivity), therefore pure Tc would not be predicted to spontaneously passivate upon exposure to pH 3.2 H_2SO_4.

Anodic polarization measurements (Figure 11, top) confirm that Tc does not passivate upon exposure to pH 3.2 H_2SO_4. A black film is observed following anodic polarization. The nature of the film will be investigated in the future, but is surmised to be $Tc(OH)_4$ based on the literature.

Although not observed on the forward scan, the reverse scan (Figure 11, bottom) indicates a transition (bend in the curve) that may be the TcO_2 / TcO_4^- transition. This

transition appears at a potential more noble than that reported in the literature (see black and red lines in Figure 10). The discrepancy may be attributable to the reported sluggishness of the TcO_2 / TcO_4^- reaction [43]. The reported data in the literature were acquired using precise methodologies and over long periods of time. The Tc / TcO_2 and TcO_2 / TcO_4^- transitions will be further investigated.

A test involving unconventional sample preparation was employed to determine whether the air-formed oxide on the surface of Tc was interfering with the formation of a passive film. The unconventional test involved polarizing a sample to -0.3V_{NHE} and abrading the surface in-situ under potential control. At -0.3V_{NHE}, Tc metal is stable and Tc oxidation is precluded. Therefore, any air-formed oxide was removed and no film would be present. Following abrasion, the sample was then polarized anodically to observe the sample behavior. Figure 12 shows the conventionally-run anodic polarization curves shown in Figure 11, along with a conventionally-run cathodic polarization curve and the unconventional prepared sample (heavy dashed line). It is seen that the behavior of the unconventionally-run sample is quite similar to those that were conventionally run. No obvious behavior differences are seen either on the cathodic branch above 0.1V_{NHE}, where Tc oxidation begins or on the anodic branch. In particular no evidence of passivity is present. One difference between the conventional and unconventional runs is a slightly higher current density in the unconventional run. This would be expected given the removal of the film which provides a mass transport barrier (as evidenced by the mass transport (i.e., non-Tafel) control upon anodic polarization).

Figure 13 includes electrochemical impedance spectra from a sample abraded in-situ at -0.5 V_{NHE}. In this set of experiments an EIS spectrum was acquired every 100 mV

up to 0.5 V_{NHE}. Samples were ramped 100 mV, followed by a 4-hour potentiostatic hold and then acquisition of an EIS spectrum. Three selected spectra are shown in Figure 13, one each from the Tc, Tc^{+4} and Tc^{+7} regions. In all cases only one time constant is apparent. Although not definitive, this is consistent with the absence of a passive film.

Figure 14 shows the results of fitting the EIS spectra acquired from the test shown in Figure 13. The model used to fit the data was the circuit shown in the top left of Figure 5. A constant phase element is used to account for the nonidealities of the surface. R_s is the solution resistance, R_p is the polarization resistance of the system and C_{dl} is the double-layer capacitance (or film capacitance) and F is the exponent which determines the phase angle of the constant phase element. The vertical dashed lines in Figures are the published Tc / TcO_2 and TcO_2 / TcO_4^- transitions along with the observed open circuit potential.

It is seen from the fitted data that there are no obvious breaks in the fitted parameters when crossing the published transition potentials. This suggests that film formation does not appear to dominate the observed cathodic reaction in the vicinity of the Tc / TcO_2 transition potential because there is no change in R_p. This also suggests that there is no significant change in the film properties when crossing the TcO_2 / TcO_4^- transition potential. All of this information supports the observation that no dramatic changes in electrochemical behavior (including passive film formation) occur in the Tc^{+4} or Tc^{+7} regions.

Our tests indicate that Tc does not follow behavior predicted by the potential – pH diagram. Neither the observed electrochemical transitions nor the presence of passivity were observed from testing.

4. SUMMARY AND OUTLOOK

To summarize, the metallic waste form degradation program utilizes a first-principles approach to enable predictive corrosion modeling of alloy waste forms, through validation with high-resolution characterizations.

(1) A multistep corrosion mechanism that is responsible for the release of Tc from any candidate alloy waste form is described, and the first-principles approach that will be used to build a predictive model for candidate alloy waste form corrosion, useful for both alloy design, and making long-term predictions is outlined.

(2) DFT modeling of Tc incorporation and transport in intermelallic oxides have started, to understand the Tc migration behavior and the structural stability in different Tc containing iron oxide forms. Future work will involve a rigorous DFT treatment that incorporates strong-electron correlations (DFT+*U*), to calculate the kinetic rates as outlined in (1).

(3) Kinetic Monte Carlo models show differences in dissolution behavior of Fe, Mo, Ni as matrix for Tc solutes. To extend to oxides, a Buckingham type pair potential for TcO_2 oxide is developed. Future work will involve the development of reactive force fields in Tc-O and Fe-Tc-O, to study oxidation and defects migration across metal/oxide interfaces, such as in the ReaxFF platform.

(4) As an initial step in assessing the viability of waste forms, technetium corrosion behavior was assessed. The films formed during electrochemical testing conditions do not show passivity. The nature of the film will be investigated in the future, but is surmised to be $Tc(OH)_4$ based on the literature. Future plan includes

electrochemical tests work across a wide range of environments (pH values) and Tc binaries (likely alloying additions include Fe, Cr, Ni and Mo).

We emphasis that this work package activity ties strongly with other experimental work on metal alloy waste form R&D, such as the Waste Form Performance Testing and Modeling (WFPTM) activity at ANL [45]. To support the Fractional Release Conceptual Model within WFPTM, the following components in this work package are considered to be important,

- Pure Tc oxidation, passivation, and Tc alloy corrosion rates in localized corrosion from modeling and electrochemical experiments
- Reactive force fields modeling of Tc transport between metal alloys and oxides
- Tc bulk incorporation mechanisms, including oxidation states in different iron oxides
- Mass transport of Tc and defects in a series of iron oxide phases

These components contribute to the passivation and oxidation rates source terms in the Conceptual Model mentioned above, providing basis for integrating waste form degradation models with performance assessment (PA) models.

5. REFERENCES

1. D. D. Keiser, D. P. Abraham, and J. W. Richardson, J. Nucl. Mater. **277**, 333 (2000).
2. J. V. Crum, D. Stachan, A. Rohatgi, and M. Zumhoff, J. Nucl. Mater. **441**, 103 (2013).
3. B. MacDougall and M. J. Graham, in *Corrosion Mechanisms in Theory and Practice*, edited by P. Marcus (Marcel Dekker, Inc., New York, 2002), p. 189.
4. D. Kolman, G. D. Jarvinen, C. D. Taylor, D. P. Moore, G. Goff, R. Gibson, M. Cisneos, E. Mausolf, P. F. Weck, E. Kim, In *Corrosion* - National Association of Corrosion Engineers: Houston, TX, 2011.
5. D. D. Macdonald, Electrochim. Acta **56**, 1761 (2011).
6. C. Y. Chao, L. F. Lin, and D. D. Macdonald, J. Electrochem. Soc. **128**, 1187 (1981).
7. L. F. Lin, C. Y. Chao, and D. D. Macdonald, J. Electrochem. Soc. **128**, 1194 (1981).
8. G. Kresse and J. Furthmüller, Comput. Mater. Sci. **6**, 15 (1996).
9. X.-Y. Liu, D. A. Andersson, and B. P. Uberuaga, J. Mater. Sci. **47**, 7367 (2012).
10. J. Hafner, C. Wolverton, and G. Ceder, MRS Bulletin **31**, 659 (2006).
11. J. K. Nørskov, F. Abild-Peterson, F. Studt, and T. Bligaard, Proc. Natl. Acad. Sci. **108**, 937 (2011).
12. O. Runevall and N. Sandberg, J Phys Condens Matter **23**, 345402 (2011).
13. I. N. Levine, *Quantum Chemistry* (Prentice HAll, Upper Saddle River, NY, 2000).
14. E. Kaxiras, *Atomic and Electronic Structure of Solids* (Cambridge University Press, Cambridge, UK, 2003).
15. C. D. Taylor, J. Phys. Chem. C, **118**, 10017 (2014).
16. B. Jeon, S. K. R. S. Sankaranarayanan, A. C. T. van Duin, and S. Ramanathan, J. Chem. Phys. **134**, 234706 (2011).
17. J. A. Martinez, D. E. Yilmaz, T. Liang, S. B. Sinnott, and S. R. Phillpot, Current Opinion Solid State Mater. Sci. **17**, 263 (2013).
18. F. N. Skomurski, K. M. Rosso, K. M. Krupka, and B. P. McGrail, Environ. Sci. Technol. **44**, 5855 (2010).
19. P. Perdew, K. Burke, and M. Ernzerhof, Phys. Rev. Lett. **77**, 3865 (1996).
20. P. E. Blochl, Phys. Rev. B **50**, 17953 (1994).
21. M. Methfessel and A. T. Paxton, Phys. Rev. B **40**, 3616 (1989).
22. H. J. Monkhorst and J. D. Pack, Phys. Rev. B **13**, 5188 (1976).
23. K. Schwochau, *Technetium: chemistry and radiopharmaceutical applications.* Wiley-VCH, 2000.
24. B. Krebs, Angewandte Chemie **8**, 381 (1969)
25. O. Muller, W. B. White, R. Roy and J. Inorg, J. Inorg. Nucl. Chem. **26**, 2075 (1964).
26. W. Schweika, A. Hoser, M. Martin, and A. E. Carlson, Phys. Rev. B **51**, 15771 (1995).
27. R. J. Lemire and D. J. Jobe , Mater. Res. Soc. **412**, 873 (1998).
28. M. E. Sherwin and T. J. Drummond. J. Appl. Phys. **69**, 8423 (1991).
29. C. Kittel, *Introduction to Solid State Physics*, 7th ed., Wiley, New York, 1996.
30. W. L. Roth, Phys. Rev. **110**, 1333 (1958).

31. A. Schrön, C. Rödl, and F. Bechstedt, Phys. Rev. B **86**, 115134 (2012)
32. M. Forti, P. Alonso, P. Gargano, G. Rubiolo, Proc. Mater. Sci. **1**, 230 (2012).
33. G. Rollmann, A. Rohrbach, P. Entel, and J. Hafner, Phys. Rev. B **69**, 165107 (2004).
34. J. Lee and S. Han, Phys.Chem. Chem. Phys. **15**, 18906 (2013).
35. P. A. Tempest and R. K. Wild, Oxidation of Metals, **23**, 207 (1985).
36. G. Henkelman, B.P. Uberuaga, and H. Jonsson, J. Chem. Phys. **113**, 9901 (2000).
37. E. Kim, P. F. Weck, C. D. Taylor, O. Olatunji-Ojo, X.-Y. Liu, E. Mausolf, G. D. Jarvinen and K. R. Czerwinski, J. Electrochem. Soc. **161(3)**, C83 (2014).
38. F. Glasso, *Structure and properties of inorganic solids*. Pergamon, New York, 1970.
39. G. Thorogood et al., Dalton Trans. **40**, 10924 (2011).
40. R. Cornell, U. Schwertmann, *The Iron Oxides: Structure, Properties, Reactions, Occurrences, and Uses* (Wiley-VCH, Weinheim, Germany), 2003.
41. S.Klotz, G. Rousse ,Th. Strässle, C. L. Bull, M. Guthrie, Phys. Rev. B **74**, 012410 (2006).
42. C. D. Taylor and X.-Y. Liu, J. Nucl. Mater. **434**, 382 (2013).
43. G. H. Cartledge, W. T. Smith, Jr., J. Phys. Chem. **59**, 1111 (1955).
44. J. W. Cobble, W. T. Smith, Jr., G. E. Boyd, J. Am. Chem. Soc. **75**, 5773 (1953).
45. J. A. Fortner and W. L. Ebert, *Status of static corrosion tests with RAW-1(Tc)*, FCRD-UFD-2012-000202.

6. FIGURES

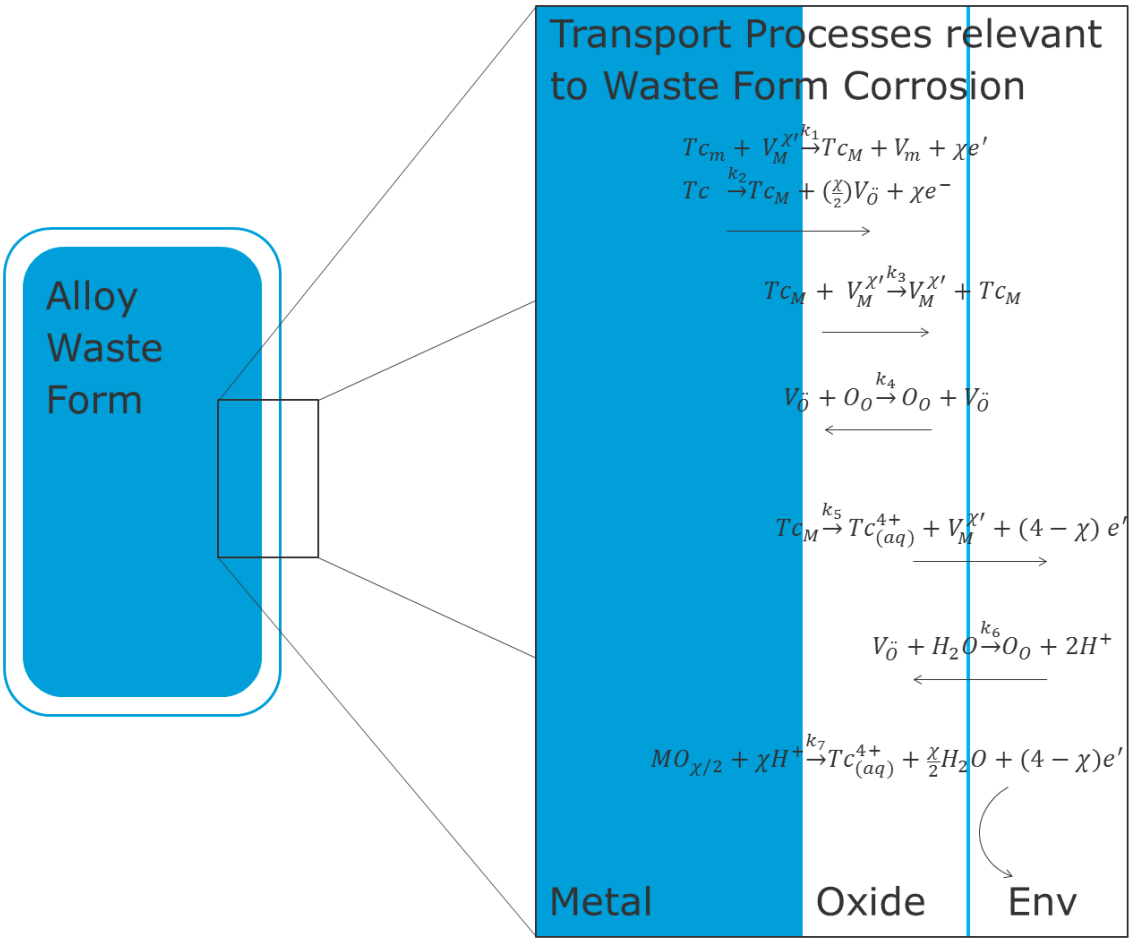

Fig. 1 Schematic of multistep processes in metal alloy waste form corrosion.

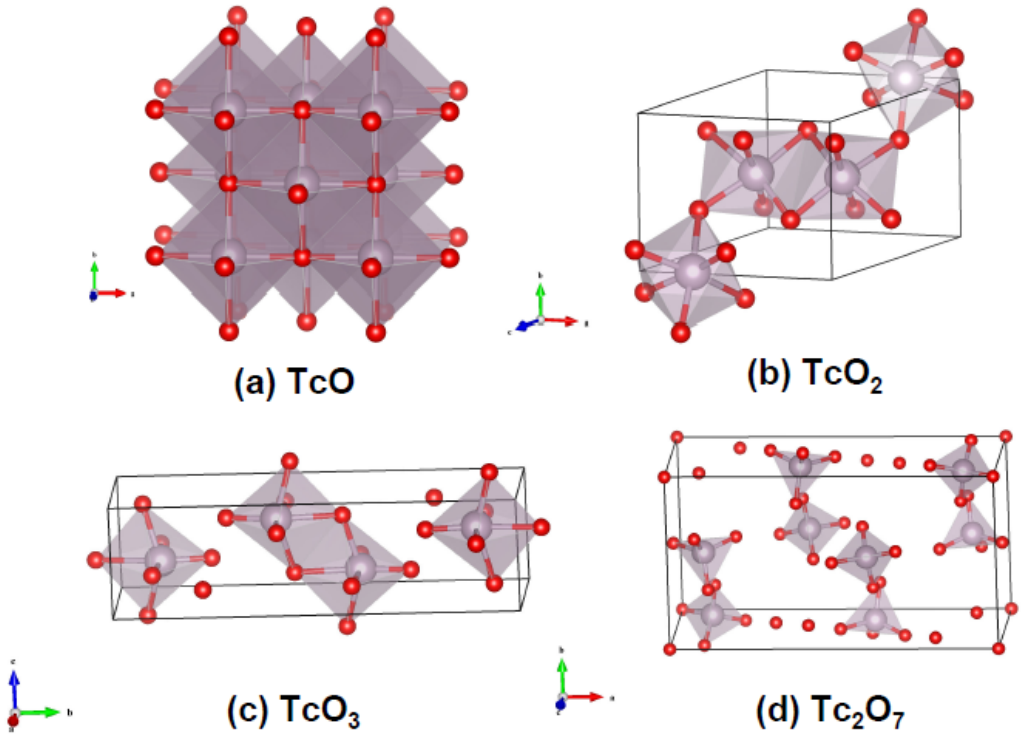

Fig. 2 Crystalline structures of binary Tc oxides: (a) TcO, (b) TcO_2, (c) TcO_3, and (d) Tc_2O_7. The grey and red spheres represent Tc and O atoms, respectively.

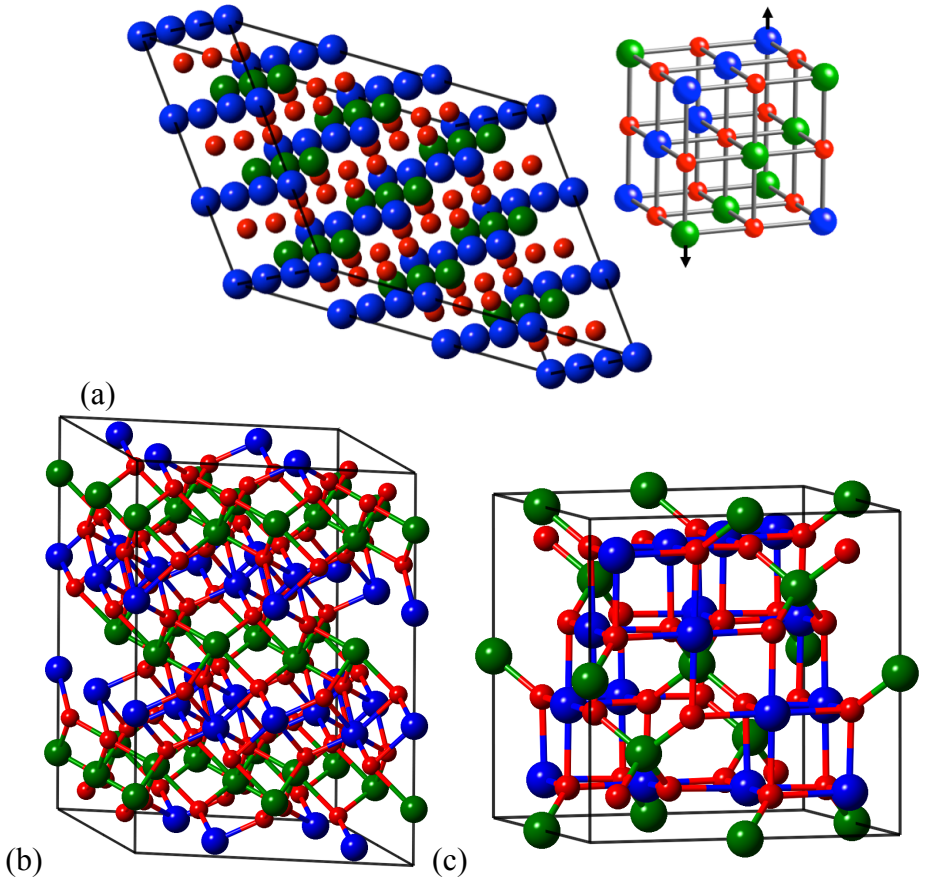

Fig. 3 Supercell structures in defects calculations (a) FeO, (b) α-Fe_2O_3, (c) Fe_3O_4. Small red balls are oxygen atoms, large blue and green balls are Fe atoms with spin up and spin down, respectively.

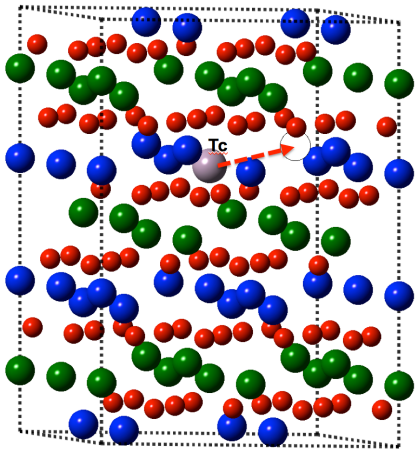

Fig. 4 Supercell structure in DFT calculation of Tc migration to a nearby Fe vacancy site in α-Fe_2O_3. Small red balls are oxygen atoms, large blue and green balls are Fe atoms with spin up and spin down, respectively.

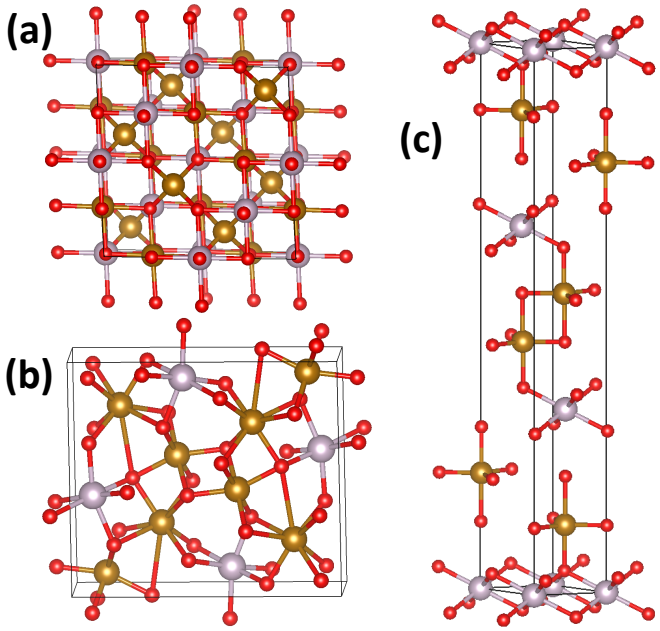

Fig. 5 Crystalline structures of Tc-Fe-O in (a) cubic (Fd-3m, 227), (b) orthorhombic (Cmcm, 63), and (c) rhombohedral (R-3m, 166) lattices. The gold, grey, and red spheres represent Fe, Tc, and O atoms, respectively.

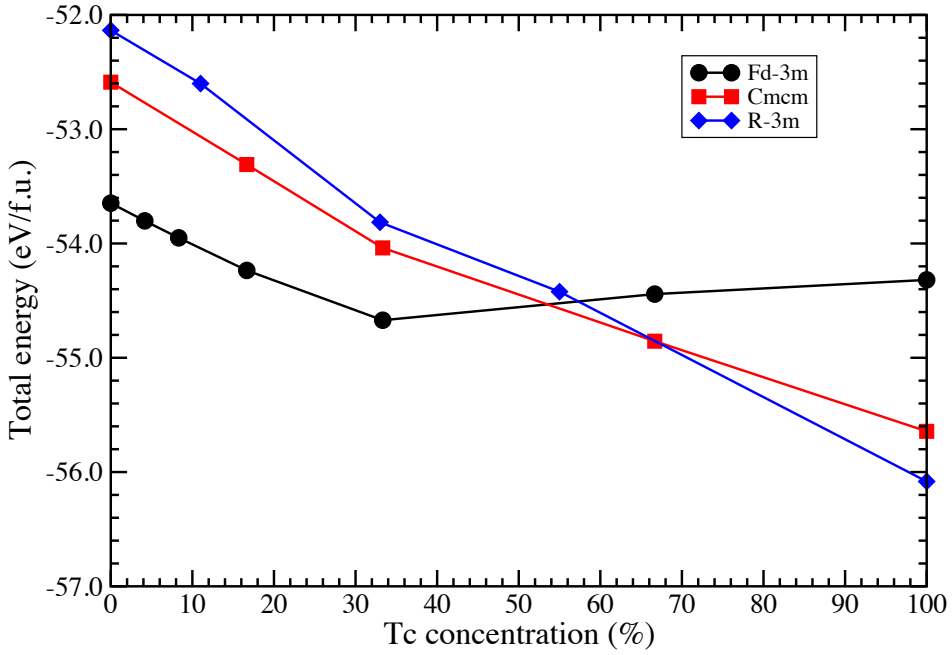

Fig. 6 Total energies of $TcFe_2O_4$ in cubic (Fd-3m), orthorhombic (Cmcm), and rhombohedral phases with respect to Tc concentration. The unit of the energy is eV per formula unit (eV/f.u.).

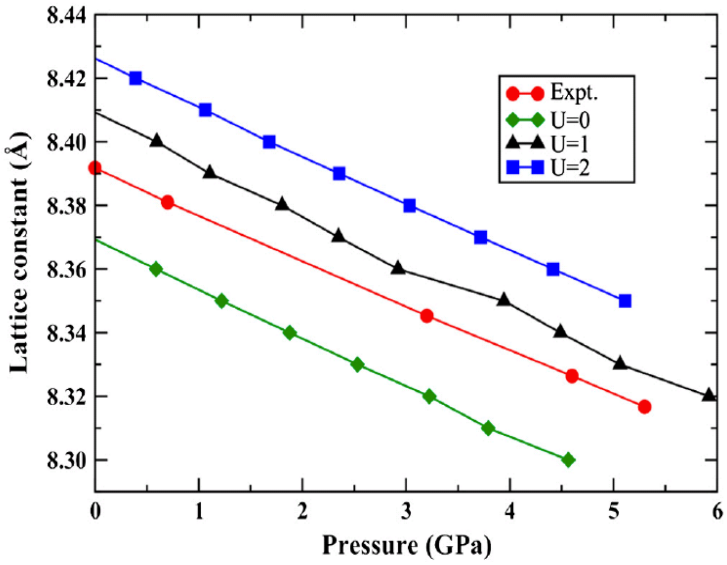

Fig. 7 Compressibility of magnetite. The experimental data were taken from Klotz et al. [41].

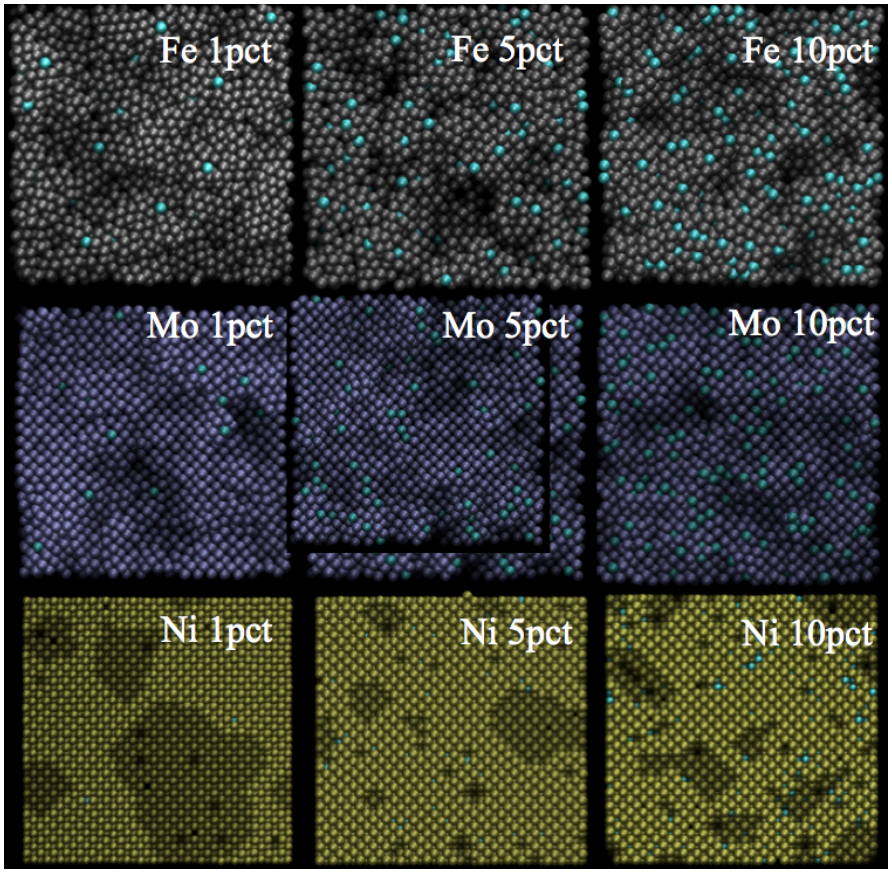

Fig. 8 Corrosion morphologies obtained as outputs after the simulation of 1000 dissolution events for candidate alloy waste forms.

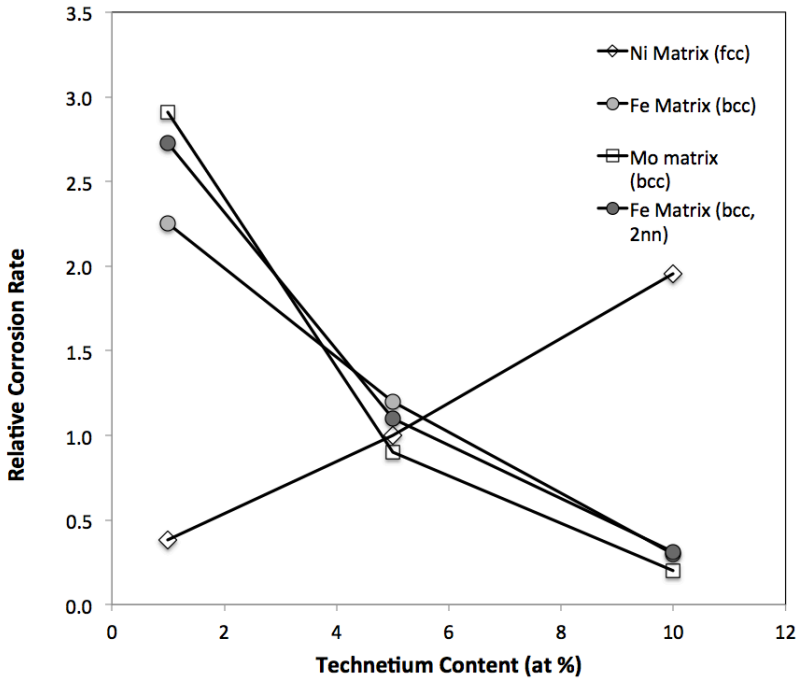

Fig. 9 Average corrosion rate versus Tc composition for Tc-Fe, Tc-Mo, and Tc-Ni.

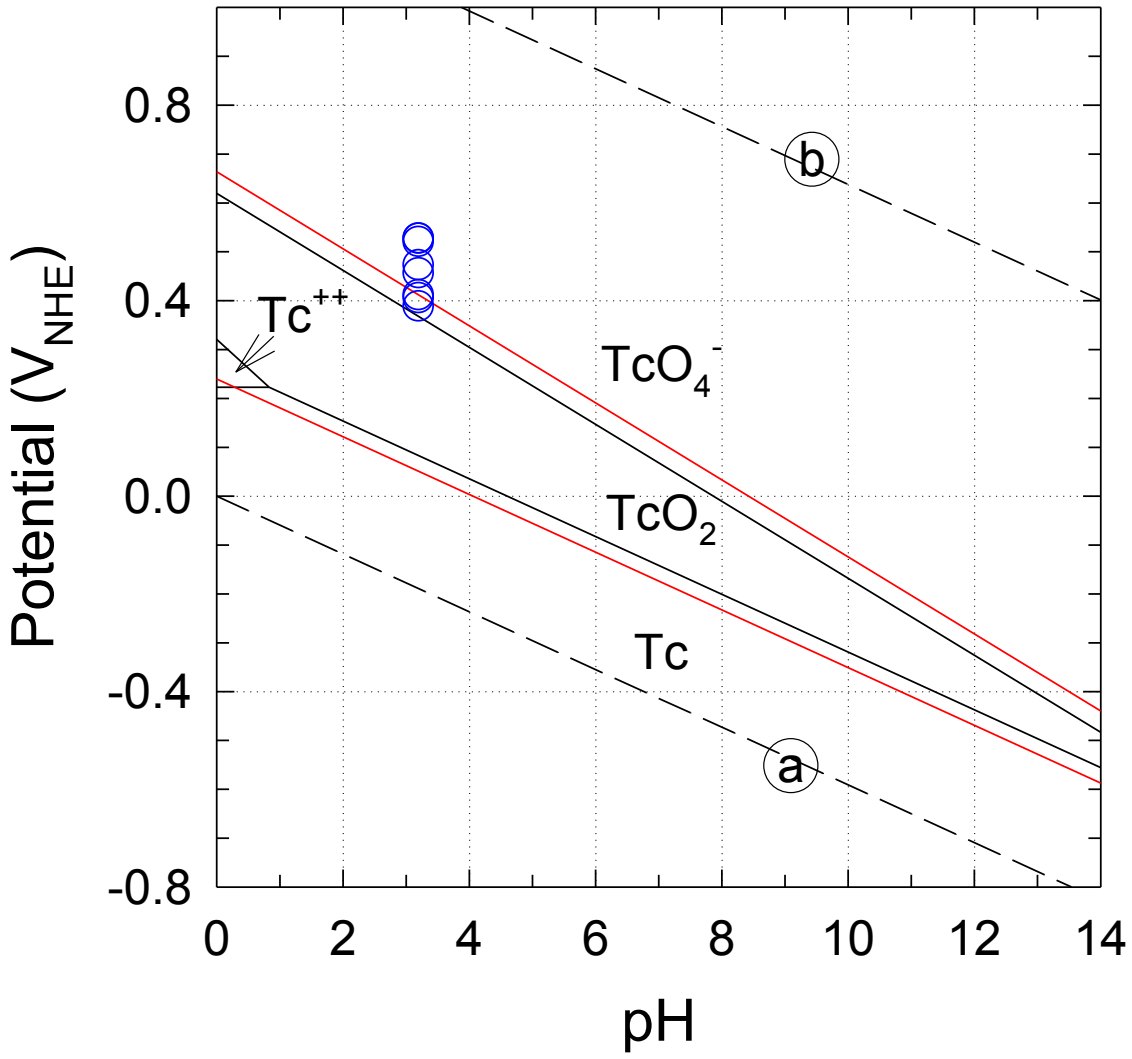

Fig. 10 Open circuit potential data following 4 hour exposure to pH 3.2 H_2SO_4. Black line – from [43]. Red line – from [44].

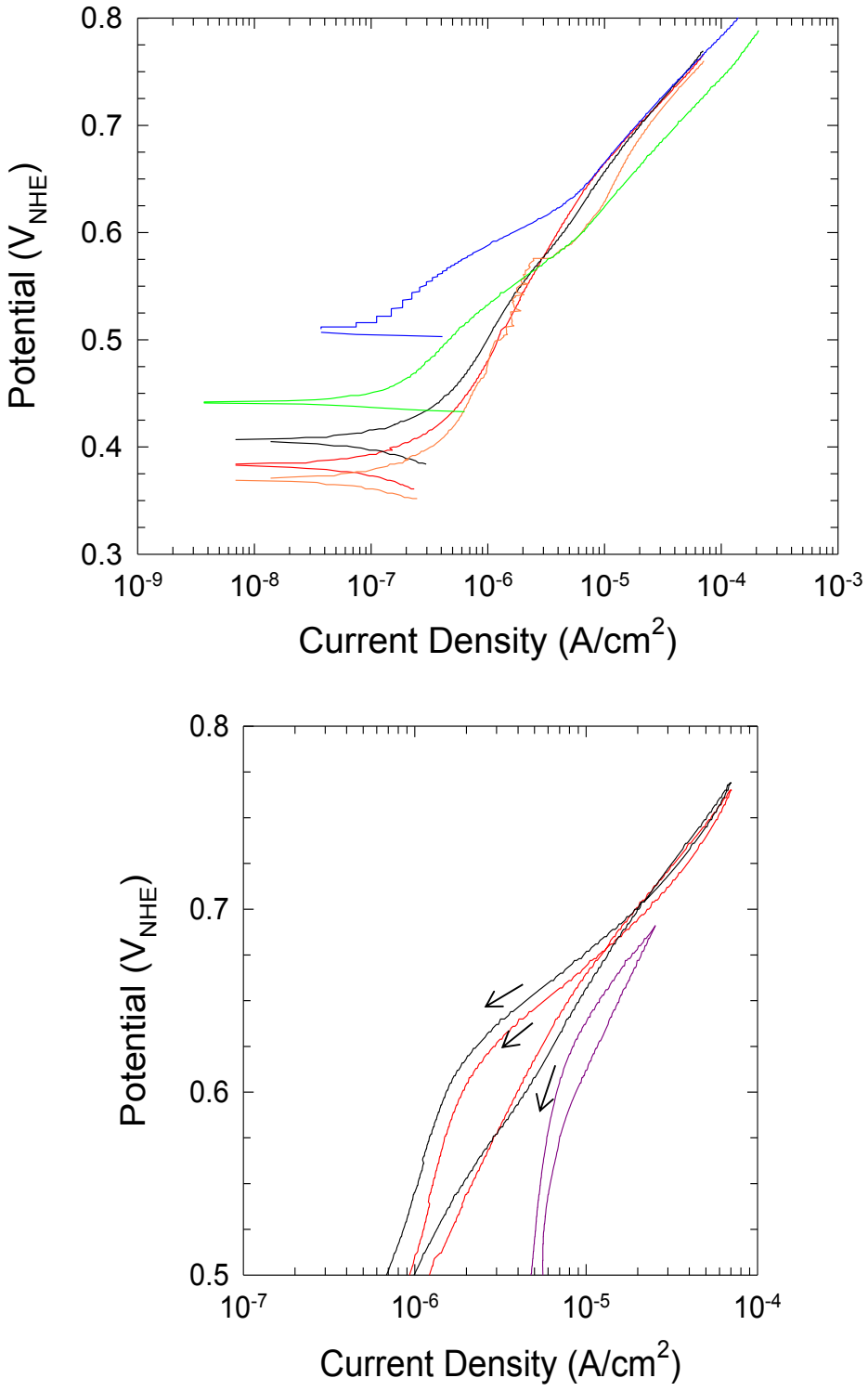

Fig. 11 Top - Anodic polarization curves for Tc exposed to pH 3.2 H_2SO_4 solution. Bottom - selected return scans.

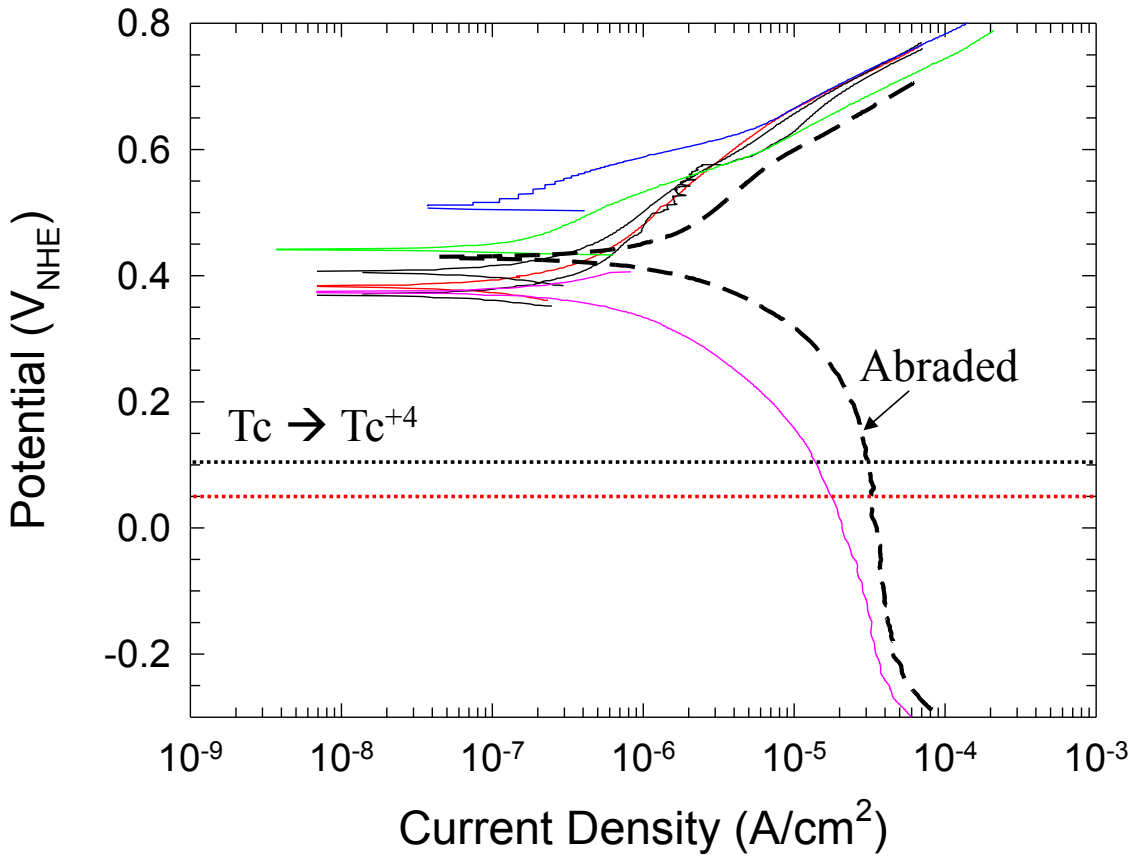

Fig. 12 Anodic and cathodic potentiodynamic polarization data. Solid lines are tests using conventionally prepared samples. The heavy dashed line is a sample abraded in-situ at $-0.3V_{NHE}$.

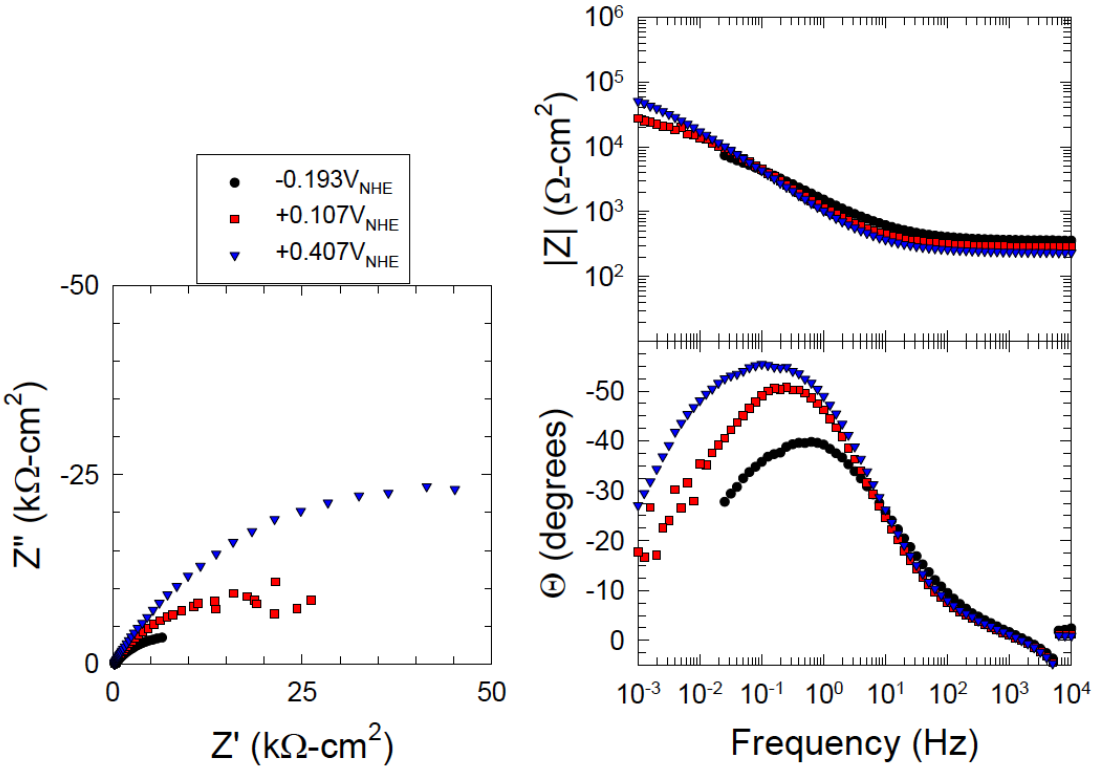

Fig. 13 Electrochemical impedance data (Nyquist (left), Bode magnitude (right top) and Bode phase angle (right bottom)) at potentials that correlate to Tc, Tc^{+4} and Tc^{+7} regions of stability. Sample was abraded at $-0.5V_{NHE}$.

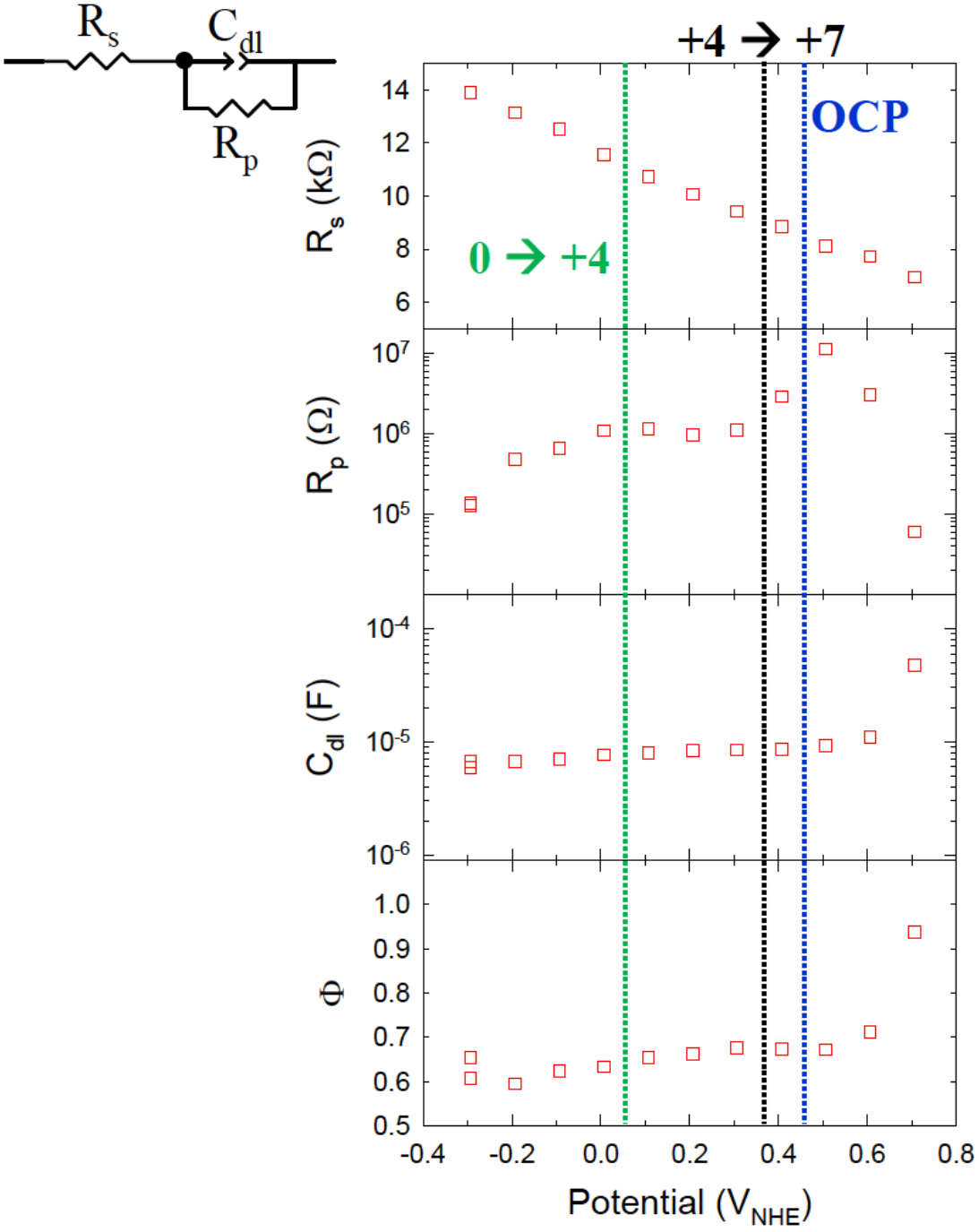

Fig. 14 Results from fitting of EIS data using the circuit model shown at the top left. OCP (open circuit potential) line is also labeled.

7. TABLES

Table 2.2.2 Structural properties of Tc, TcO_2 and Tc_2O_7. Units are in Å and eV per formula unit (eV/f.u) for the lattice constants and formation energy, respectively. Experimental values are from references: a: Ref. [29], b: Ref. [25,27], and c: Ref. [24,25].

	Tc (HCP)		TcO_2 (Monoclinic)		Tc_2O_7 (Orthorhombic)	
	DFT	Expt. [a]	DFT	Expt. [b]	DFT	Expt. [c]
Lattice constant (Å)	a=2.75 c =4.40	a=2.74 c=4.40	a=5.77 b=4.86 c=5.65	a=5.53 b=4.79 c=5.53	a=15.09 b=8.19 c=6.19	a=13.76 b=7.44 c=5.62
Formation energy (eV/f.u.)	6.97	6.85	4.25	4.75	10.88	11.53

Table 2.2.3 Spin-polarized PAW-PBE DFT calculated relative energy for different Fe vacancies, and Tc incorporation energy at available Fe vacancy sites in FeO, α-Fe_2O_3, and Fe_3O_4.

	FeO	α-Fe_2O_3	Fe_3O_4	
			Octahedral	Tetrahedral
Relative energy for different Fe vacancies (eV)	N/A	N/A	0.0	-37.15
Tc incorporation energy (eV)	3.10	-3.11	-39.40	50.95

Table 2.2.5 Lattice constant and bulk modulus of magnetite. Units are in Å and GPa for the lattice constant and bulk modulus, respectively.

U_{eff} (eV)	0	2	4	Expt. [41]
Lattice constant (Å)	8.37	8.43	8.45	8.39
Bulk modulus (GPa)	173	176	178	180